Journal of Materials Chemistry A

Accepted Manuscript

ROYAL SOCIETY OF CHEMISTRY

www.rsc.org/materialsA

Journal Name

ARTICLE

Interfacial Reaction-Directed Synthesis of Ceria Nanotube-embedded Ultra-small Pt Nanoparticle Catalyst with High Catalytic Activity and Thermal Stability†

Received 00th January 20xx,
Accepted 00th January 20xx

DOI: 10.1039/x0xx00000x

www.rsc.org/

Yong Wang,[a] Guolong Song,[a] Zhenhe Xu,[b] Federico Rosei,[b] Dongling Ma[b] and Guozhu Chen*[a]

A catalyst based on ceria nanotube-embedded ultra-small Pt nanoparticles was synthesized by means of an interfacial reaction in the absence of any surfactants and without involving any separate surface modification process. When $Ce(OH)CO_3$ nanorods and H_2PtCl_6 are introduced into a NaOH aqueous solution in sequence, a solid-liquid interfacial reaction between $Ce(OH)CO_3$ and NaOH occurs. The formed $Ce(OH)_3$ then deposits on the external surface of $Ce(OH)CO_3$ nanorods. During the interfacial reaction, the negatively charged Pt species is expected to be electrostatically attracted to gradually formed $Ce(OH)_3$ due to its positive charge, resulting in a uniform mixture of Pt species and $Ce(OH)_3$. After removing residual $Ce(OH)CO_3$ and hydrogen reduction, ceria nanotube-embedded Pt nanoparticle hollow composites were achieved. Due to the ultra-small size of catalytically active Pt nanoparticles and the close contact between Pt and ceria, the catalyst exhibits high catalytic activity toward CO oxidation and excellent thermal stability even at temperatures as high as 700 °C, suggesting that they also hold promise for higher temperature catalytic reactions.

1. Introduction

The catalytic properties of noble metal based composites are strongly dependent on the type of support, size of noble metal particles and their structural details.[1–6] Because of its excellent oxygen releasing/uptaking capacities, ceria (CeO_2) is considered as one of the most important supports, not only for stabilizing catalytic noble metal particles but also for inducing the synergistic effect between particles and supports in some catalytic reactions.[7–13] So far, to achieve high efficiency CeO_2-noble metal catalysts, significant efforts have been expended on the synthesis of morphology-controllable CeO_2 support and the size-tunable production of noble metal particles.[1,12,14,15]

Due to its high surface area, hollow structured CeO_2 is expected to facilitate the dispersion of noble metal nanoparticles (NPs)[16–22] and favor passage of reactant molecules to the active sites of the catalysts. In the case of supported noble metal NPs, the reduction of their size is generally regarded as an efficient way to increase their catalytic activity.[23] However, in real-world applications, these catalysts are often required to work at relatively high temperature. The ensuing collapse of the hollow structured support and sintering of the noble metal NPs thus become major issues, leading to a decreased catalytic activity.[24,25] From this viewpoint, the construction of CeO_2-noble metal composites with high catalytic activity and superior thermal stability represents a technologically crucial yet challenging problem.[26]

CeO_2-noble metal composites are demonstrated to be suitable catalysts for CO oxidation, which is regarded as one of the hottest topics in the field of catalysis because it is an essential step in industrial reactions as well as its environmental impact. In order to improve the catalyst activity as well as thermal stability, one can confine noble metal NPs into mesoporous CeO_2[4] or modify CeO_2 support with doping.[13] Although these strategies can solve the issues stated above to some extent, they cannot completely avoid the migration and sintering of noble metal NPs.[1] Recently, encapsulating noble metal NPs into hollow structured CeO_2 has been shown to be an ideal architecture to suppress the sintering of noble metal NPs, and thus enabling them to retain good catalytic activity towards CO oxidation even after high temperature thermal treatment.[27] Representative work was reported by Xia's group, where they deposited polyvinylpyrrolidone-capped Pt NPs on plasma treated polystyrene fibers, followed by CeO_2 coating.[28] After removing the polystyrene fibers by calcination, Pt NPs were successfully embedded in CeO_2 hollow fibers. Due to the intimate contact between CeO_2 and Pt, the catalyst could resist thermal sintering up to 700 °C without structural collapse.[28] Zheng's group also found that the Pd@CeO_2 multi-yolk-shell catalyst exhibited high catalytic activity towards CO oxidation and thermal stability even after treatment at 550 °C for 6 h, demonstrating that a multi-core-shell structure can prevent the aggregation of fine Pd NPs.[29] Although much progress has been achieved in the construction of CeO_2-noble metal hollow composites, this is a multistep process that requires complex surface modification with the assistance of surfactants and

[a] School of chemistry and chemical engineering, University of Jinan, Jinan, Shandong province, 250022 (China), Email: chm_chengz@ujn.edu.cn
[b] Institut National de la Recherche Scientifique, 1650 Boulevard Lionel Boulet, Varennes, Québec, J3X 1S2 (Canada)
† Electronic Supplementary Information (ESI) available: See DOI: 10.1039/x0xx00000x

precise control on coating, thereby limiting their large-scale synthesis and practical applications. Generally speaking, developing facile and environmentally friendly strategies for the synthesis of CeO_2-noble metal hollow composites is still a key challenge.

In previous work, we chose $Ce(OH)CO_3$ nanorods as template and successfully fabricated CeO_2-based nanotubes through interfacial reactions.[16,30–32] Upon the addition of $Ce(OH)CO_3$ into basic solution, the formed $Ce(OH)_3$ preferentially nucleates on the $Ce(OH)CO_3$ surface. Since $Ce(OH)_3$ is easily transformed into CeO_2, hollow structured CeO_2 can be obtained once the residual $Ce(OH)CO_3$ is removed by etching with acid. Herein, we extend the use of $Ce(OH)CO_3$ nanorods to synthesize CeO_2-Pt nanotube composites via a simple interfacial reaction. Upon the addition of $Ce(OH)CO_3$ nanorods and H_2PtCl_6 into a NaOH aqueous solution in sequence, followed by acid-washing and hydrogen treatment, a CeO_2 nanotube-embedded ultra-small Pt NP catalyst can be easily synthesized in the absence of any surfactants and without any specific surface modification (Scheme 1). Due to the intimate contact between Pt and CeO_2, ultra-small size of Pt and hollow structure of the composites, the resulting CeO_2-Pt nanotubes exhibit high catalytic activity towards CO oxidation at low temperature. Importantly, the as-prepared catalysts display excellent thermal stability even at temperatures as high as 700 °C and this kind of structure restrains the sintering of both Pt and CeO_2 NPs.

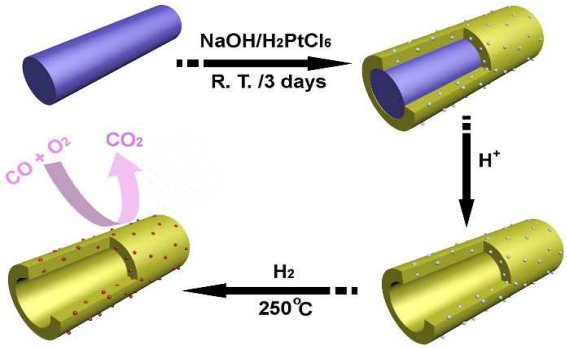

Scheme 1 Schematic illustration of the facile synthesis of hollow CeO_2-Pt nanostructure.

2. Results and discussion

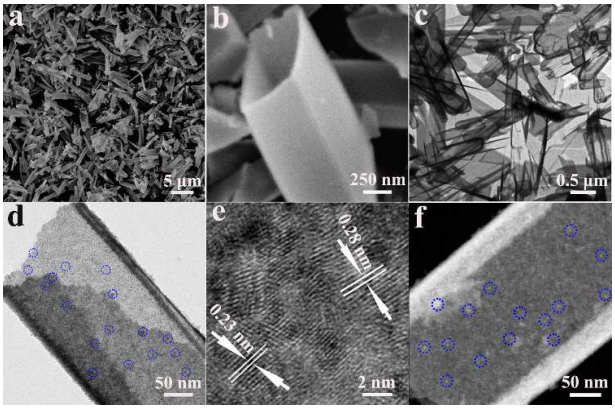

Fig. 1 a), b) SEM images, c), d) TEM images, and e) HRTEM image, f) HAADF-STEM image of the CeO_2-Pt composite. Blue dashed circles in d) and f) highlight Pt NPs.

As shown in Fig. 1a, the as-prepared sample resembles the size of the $Ce(OH)CO_3$ nanorod template.[30–32] In particular the quadrangular shape can be clearly visualized from the cross-section of one nanotube with typical wall thickness of around 40 nm (Fig. 1b). The sharp contrast between the edge and center parts of these one-dimensional structures is clearly visible in low-magnification TEM imaging (Fig. 1c), similarly to our previous report.[16,30–32] However, in this case there are some distinguishable, ultra-small Pt NPs (denoted by dashed circles in Fig. 1d) that are separately embedded in the nanotube wall. The measured d spacing of ~0.23 nm in the HRTEM images (Fig. 1e and Fig. S1†) is assigned to the lattice spacing of the (111) plane of Pt, and the interlayer distance of ~0.28 nm can be indexed to the lattice spacing of the (200) plane of CeO_2. The CeO_2 nanotube-embedded ultra-small Pt NPs were further characterized by Scanning Transmission Electron Microscopy (STEM), where the brighter spots correspond to Pt NPs (Fig. 1f). This synthetic strategy does not require either additional surface modification process or the use of any stabilizing molecules, which is advantageous from the synthesis point of view.

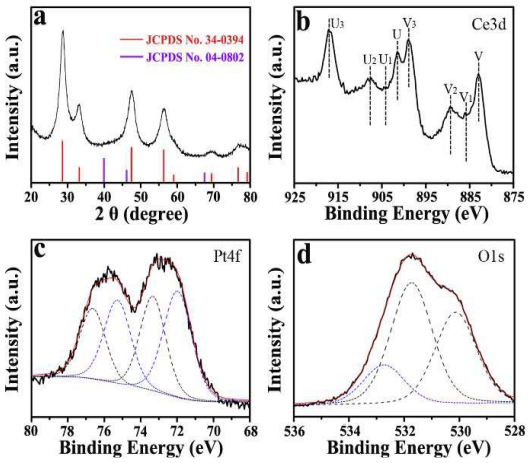

Fig. 2 a) XRD pattern of CeO_2-Pt. XPS spectra of (b) element Ce, (c) element Pt and (d) element O in CeO_2-Pt.

Characterization by X-ray diffraction (XRD) was performed to study the crystalline structure of the nanotubes. As shown in Fig. 2a, all diffraction peaks could be well indexed to fluorite-phase CeO_2 (JCPDS No. 34-0394) and no obvious diffraction peaks of Pt could be detected, which should result from the ultra-small size and uniform distribution of embedded Pt NPs. The valence states of Ce, Pt and O were determined by X-ray photoelectron spectroscopy (XPS). As shown in Fig. 2b, the Ce 3d electron core level is characterized by two series of peaks: 3d5/2 and 3d3/2. The peaks labeled "V" are associated with Ce 3d5/2, and those labeled with "U" pertain to Ce 3d3/2. Specifically, the peaks labeled with U, U2, U3 and V, V2, V3, are characteristic of Ce(IV), while the peaks U1 and V1 are

characteristic of Ce(III), indicating that Ce(III) co-exists with Ce(IV) in the as-prepared CeO_2. In the case of the Pt 4f core level spectrum (Fig. 2c), the peaks are deconvoluted into two components: the peaks centered at 71.9 and 75.2 eV can be assigned to the metallic(0) Pt 4f7/2 and Pt 4f5/2.[12,33–37] The peaks at 73.3 and 76.6 eV can be attributed to Pt(II) species, which may be due to the electron transfer from Pt atoms to CeO_2 arising from the strong interfacial effect.[38,39,41] The relatively high intensity of these peaks further corroborated the high dispersity of ultra-small Pt NPs in CeO_2, which maximized the contact between Pt and CeO_2. In the O1s XPS spectrum (Fig. 2d), the peaks at ~530.1, 531.7 and 532.7 eV correspond to the lattice oxygen in CeO_2, the chemisorbed oxygen and weakly bonded oxygen species, respectively.[14] The concentration of Pt in the CeO_2-Pt nanotubes was ~4.6 wt%, as determined by inductively coupled plasma mass spectrometry (ICP-MS).

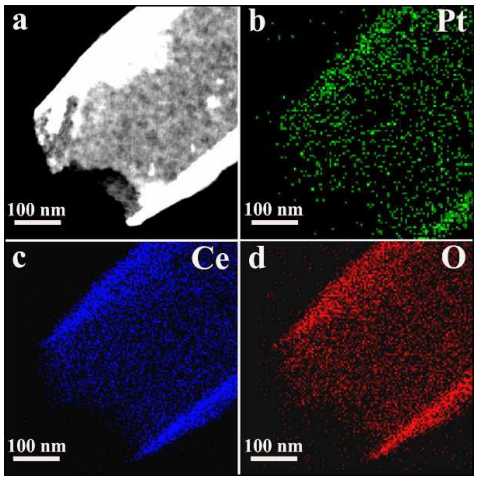

Fig. 3 HAADF-STEM image (a), and Pt (b), Ce (c) and O (d) STEM-EDX maps of an individual CeO_2-Pt nanotube.

The co-existence of Ce and Pt in the as-prepared sample was also supported by Energy Dispersive X-Ray Spectroscopy (EDX) measurements, whereby both Ce and Pt signals were detected from the same nanotube (Fig. S2†). To investigate the elemental distribution of Pt in the nanotubes, High Angle Annular Dark Field (HAADF)-STEM images and elemental maps were acquired on an individual nanotube (Fig. 3). Elements Pt, Ce, and O are evenly distributed throughout the nanotube, revealing that the ultra-small Pt NPs are homogeneously dispersed in the nanotubes. Such uniform distribution of Ce and Pt is highly beneficial to strengthen the interaction between CeO_2 and Pt NPs, and is expected to render the embedded Pt NPs thermally stable.

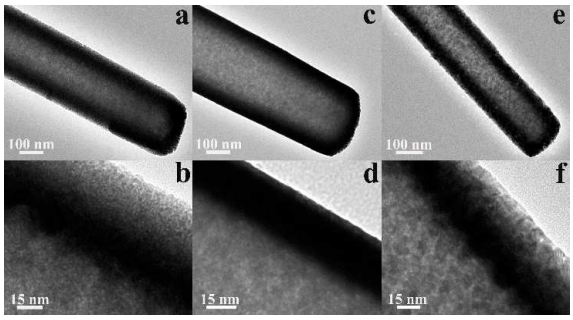

Fig. 4 a), c), e) Low-magnification TEM images showing three individual CeO_2-Pt nanotubes after they were calcined in air for 2 h at a) 500, c) 700 and e) 800 °C, respectively. b), d), f) High-magnification TEM images revealing the wall structures of the CeO_2-Pt after calcination in air for 2 h at b) 500, d) 700, and f) 800 °C.

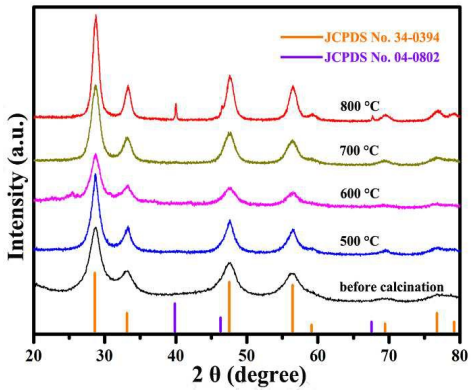

Fig. 5 XRD patterns of CeO_2-Pt nanotube composites before and after calcination in air at 500, 600, 700, and 800 °C for 2 h.

We propose that the combination of interfacial reaction and co-precipitation is responsible for the formation of CeO_2 nanotube-embedded Pt NPs. As shown in Scheme 1, when $Ce(OH)CO_3$ nanorods and H_2PtCl_6 are introduced into a NaOH aqueous solution in sequence, a solid-liquid interfacial reaction occurs between $Ce(OH)CO_3$ and NaOH. The $Ce(OH)CO_3$ nanorod, being a sacrificial template, slowly dissociates Ce^{3+} ions, reacting with OH^- to form $Ce(OH)_3$ on the external surface of $Ce(OH)CO_3$ nanorods. Meanwhile, the ligand exchange reaction of Cl^- in H_2PtCl_6 by OH^- is kinetically slow,[40] which is reflected from the gradual decrease of Pt concentration in solution with time (Fig. S3†). Thus, the formed $[Pt(OH)_xCl_y]^{m-}$ species is supposed to be electrostatically attracted to positively charged $Ce(OH)_3$,[3] resulting in analogous co-precipitation and a good blend of Pt species and $Ce(OH)_3$ during the interfacial reaction. After the removal of residual $Ce(OH)CO_3$ and hydrogen reduction, the CeO_2 nanotube-embedded Pt NP hollow composites are achieved. This method can also be extended to prepare CeO_2 nanotubes embedded Ru NPs (Fig. S4†), when H_2PtCl_6 is replaced by $RuCl_3$.

The as-prepared samples were heat-treated at different temperatures to probe their thermal stability. As shown in Fig. 4 and Fig. S5†, all samples that were calcined at 500~800 °C in air for 2 h still maintained a tubular structure with a diameter of 300-500 nm, inheriting the dimensions of the $Ce(OH)CO_3$ template and keeping the tube shape of uncalcined CeO_2 (Fig.

1c) without collapse. Pt NPs were still hard to distinguish even when the sample was calcined up to 700 °C, demonstrating that the ultra-small Pt NPs were effectively prevented from sintering. When the sample was treated at 800 °C, Pt NP can be clearly visualized (Fig. S6†). The sinter-resistant sample was further characterized by XRD. As shown in Fig. 5, there was no obvious diffraction peak width change of CeO_2 and no diffraction peaks indexed to Pt for the samples treated at 500, 600 and 700 °C, indicating that both CeO_2 and Pt exhibit a good thermal stability. After treatment at 800 °C, one diffraction peak at 39.6° that is indexed to Pt (111) appears because of the sintering of Pt NPs at this temperature, which is consistent with TEM results. The crystallite size for pure CeO_2 nanotubes increases from ~6.1 nm at 500 °C to 11.4 nm at 800 °C, in comparison to ~5.3 nm at 500 °C to 7.1 nm at 800 °C in the case of CeO_2-Pt nanotube composites. This indicates that the CeO_2 nanotube-embedded ultra-small Pt NP structure increases the sinter-resistant capacity of Pt NPs and simultaneously restrains CeO_2 sintering (Fig. S7† and Table S1†). The good thermal stability of the as-prepared CeO_2-Pt nanotube composite catalyst is further demonstrated by thermal gravity (TG) curve, where there is no much weight loss in the range of 200~850°C (Fig. S8†).

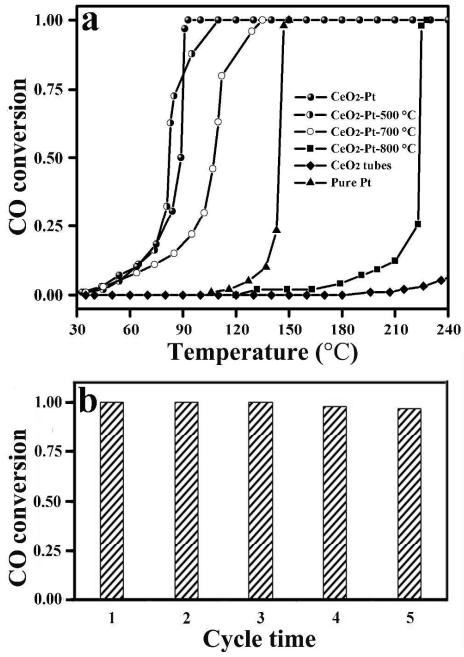

Fig. 6 a) CO conversion curves of CeO_2 tubes, pure Pt, and CeO_2-Pt before and after calcination in air at 500, 700 and 800 °C for 2 h. b) catalytic cycles of the as-prepared uncalcined CeO_2-Pt catalyst at 115 °C.

Here, the CO oxidation reaction was selected as a model reaction to evaluate the catalytic activity and thermal stability of the as-prepared CeO_2 nanotube embedded ultra-small Pt NP catalyst. As shown in Fig. 6a, complete oxidation was achieved over the as-prepared sample at around 80 °C, far more active than either pure Pt or pure CeO_2. The calculated reaction rate reaches 36.9 μmol g^{-1} s^{-1}, which is higher than most reported CeO_2 supported Pt catalysts (Table 1). Arrhenius plots show that the activation energy of the as-prepared catalyst is around 49.8 kJ mol^{-1} (Fig. S9†), which is also comparable to other values reported (Table 1). The high catalytic activity could be attributed to the ultra-small size of Pt NPs, and high specific surface area (~62.3 m^2/g) (Fig. S10†) of the hollow structured catalyst with permeable shell (Fig. S11†). During the CO oxidation reaction, this kind of structure favors diffusion and transportation of reactant molecules to the CeO_2 and Pt more effectively. In addition, the synergistic effect between CeO_2 and Pt should be also taken into account. It is recognized that the Pt cations at the CeO_2-Pt interface can result in relatively weak Pt-CO bonds and enhanced oxygen reducibility during CO oxidation reaction.[41] The synergistic effect is also inferred from H_2 temperature-programmed reduction (H_2-TPR) results, where the H_2 consumptions below 100 °C were attributed to the reduction of oxygen close to the CeO_2-Pt interface (Fig. S12†). After thermal treatment at 500 °C, there is no obvious decrease in activity with complete CO oxidation at ~100 °C. Even when treated at high temperature up to 700 °C, the catalyst still displayed a very high catalytic activity, with reaction rate 28.3 μmol g^{-1} s^{-1}, further demonstrating that this unique structure of the catalyst (well mixed CeO_2 and Pt nanostructures in the wall of nanotubes) can prevent migration and sintering of Pt NPs at elevated temperature. To study the durability of the CeO_2-Pt catalyst, the used product was continuously tested under the same CO oxidation conditions. It was found that after five catalytic cycles at 115 °C (Fig. 6b) or even 160°C (Fig. S13†), the as-prepared uncalcined CeO_2-Pt catalyst still maintained almost 100% conversion rate of CO into CO_2, indicating that the as-prepared CeO_2-Pt nanotube catalyst has a good durability.[3,28]

Table 1 Comparative study of different Pt/CeO_2 catalysts.

Catalyst		T (range) (°C)	Rate (r) (mmol g^{-1} s^{-1})	Activation energy (Ea) (kJ mol^{-1})	Reference
Pt-CeO_2	Tube	33-93	0.0369 (63 °C)	49.8	This study
Pt-CeO_2(500 °C)	Tube	34-110	0.0369 (63 °C)	59.32	This study
Pt-CeO_2(700 °C)	Tube	35-150	0.0283 (63 °C)	34.3	This study
Pt-CeO_2	Rod	27-160	0.00346 (80 °C)	34 ± 2	Ref. [14]
	Cube	27-180	0.00303 (80 °C)	46 ± 2	Ref. [14]
	Octahedra	27-190	0.000795 (80 °C)	63 ± 4	Ref. [14]
Pt-CeO_2	Rod	170-230	Not stated	145	Ref. [42]
	Octahedra			101	Ref. [42]
Pt-CeO_2	Lamella	220-330	Not stated	Not stated	Ref. [43]
Pt-CeO_x		100-350	0.0204	85.4	Ref. [44]
Pt-CeO_2/Al_2O_3		90-210	Not stated	43	Ref. [45]
Pt-CeO_2		50-300	Not stated	44	Ref. [46]

3. Conclusions

In summary, a CeO_2 nanotube embedded Pt NP catalyst was successfully fabricated by easily reacting the $Ce(OH)CO_3$ template and H_2PtCl_6 with NaOH aqueous solution, followed by removal of the residual template. The ultra-small Pt NPs embedded in the walls of CeO_2 nanotubes were shown to be a unique, highly beneficial structural feature, both enhancing the contact between Pt and CeO_2, and preventing the sintering Pt NPs and CeO_2 alike. As a result, the CeO_2 nanotube embedded Pt NP catalyst exhibits high catalytic activity towards CO oxidation and could resist thermal treatments up to 700 °C without sintering, a feature of high stability. The developed synthetic route is simple albeit efficient and can be easily extended to fabricate CeO_2 nanotubes embedded other noble metal NPs, e.g. Ru, and also can be potentially extended to the synthesis of noble metal NP embedded other hollow structure when suitable templates are chosen. The designed structure well balances activity and stability of noble metal NPs, thus would serve as excellent model in high temperature catalytic reactions from the both theoretical and practical perspectives.

4. Experimental Section

4.1 Chemicals

Cerium(III) nitrate hexahydrate ($Ce(NO_3)_3{\cdot}6H_2O$), urea ($CO(NH_2)_2$), sodium hydroxide (NaOH), chloroplatinic acid ($H_2PtCl_6{\cdot}6H_2O$), nitric acid (HNO_3) were of analytical grade and were used as received from Sinopharm Chemical Reagent Co. Ltd. All solutions were prepared using deionized water (resistance >18 MΩ cm).

4.2 Synthesis of $Ce(OH)CO_3$ templates

In a typical experiment, $Ce(NO_3)_3{\cdot}6H_2O$ (4 mmol) and urea (24 mmol) were added to 80 mL water under vigorous magnetic stirring at 80 °C for 24 h. The obtained powder sample was centrifuged, washed with distilled water and dried.[31]

4.3 Synthesis of CeO_2-Pt

Under nitrogen atmosphere 100 mg of prepared $Ce(OH)CO_3$ was dispersed in 30 mL of NaOH aqueous solution (3 M) at room temperature. After stirring for 10 min, 1.0 mL of aqueous $H_2PtCl_6{\cdot}6H_2O$ (0.01 g mL^{-1}) solution was added with constant slow stirring. Then the resulting solution was continuously stirred for 24 h and kept undisturbed for 2 days. Subsequently, the sample was thoroughly washed with ultrapure water and dried at 80 °C. Next, the sample was thoroughly washed using HNO_3 (1 M) to remove unreacted templates, and dried at 80 °C. Finally, as-dried samples were reduced in a gaseous mixture of H_2 and N_2 (1/9, v/v) for 1 h at 250 °C with a heating rate of 3 °C min^{-1}, and the resulting catalysts were denoted as CeO_2-Pt. The pure Pt NPs were prepared by reducing H_2PtCl_6 in liquid phase with strong reductant $NaBH_4$.

4.4 Materials characterization

The as-prepared samples were characterized by X-ray powder diffraction (XRD) using a Japan Rigaku D/Max-γA rotating anode X-ray diffractometer equipped with Cu Kα radiation (λ = 1.54178 Å) in the 2θ range from 20 to 80°. The morphology and structure of the samples were studied using a field emission scanning electron microscope (FE-SEM) (JSM-6700F), transmission electron microscope (TEM) (JEM-2100) equipped with an Energy Dispersive X-Ray Spectroscopy (EDX), and X-ray photoelectron spectrometer (XPS) with Al Kα radiation. The Pt content in the CeO_2-Pt sample was determined using an inductively coupled plasma mass spectrometer (ICP-MS, Thermo Scientific XSeries-2). N_2 adsorption–desorption isotherms were measured at 77 K on a Micromeritics TriStar II 3020 surface area & pore size analyzer. Before measurement, the samples were outgassed in a vacuum at 300 °C for 4 h. The Brunauer–Emmett–Teller (BET) method was used to calculate the surface areas of the samples. The pore size distributions were derived from the desorption branches of the isotherms using the Barrett–Joyner–Halenda (BJH) method. TG analysis was performed in the temperature range of 25-850°C and at a heating rate of 10°C/min in Ar atmosphere.

Hydrogen temperature-programmed reduction (H_2-TPR) of the samples was carried out in a conventional flow system

equipped with a thermal conductivity detector. 50 mg of sample was used and pretreated in a 5% O_2/N_2 flow (40 mL min^{-1}) at 400 °C for 30 min. After the sample was cooled down to room temperature, a 10% H_2/N_2 mixture gas (40 mL min^{-1}) was introduced and the reactor was heated at a rate of 10 °C min^{-1} from room temperature to ~300 °C.

Catalytic activity was measured using a continuous flow fixed-bed micro-reactor at atmospheric pressure. In a typical experiment, the system was first purged with high purity N_2 gas and then a gas mixture of $CO/O_2/N_2$ (1: 10: 89) was introduced into the reactor which contained 20 mg samples at a flow rate of 50 mL min^{-1}. Gas samples were analyzed with an online infrared gas analyzer (Gasboard-3100, China Wuhan Cubic Co.). For durability test, the used sample was purged with N_2 and cooled down to room temperature. Subsequently it was re-tested under the same CO oxidation conditions described above.

Acknowledgements

This work was supported by the Shandong Provincial Natural Science Foundation, China (Grant No. ZR2015BM008), Scientific Research Foundation for the Returned Overseas Chinese Scholars, State Education Ministry. Financial support from the Natural Sciences and Engineering Research Council of Canada (D.M. and F.R.) is also appreciated. F.R. acknowledges an EWR Steacie Memorial Fellowship and the Canada Research Chairs program for partial salary support.

Notes and references

1 J. Qi, J. Chen, G. Li, S. Li, Y. Gao and Z. Tang, *Energy Environ. Sci.* 2012, **5**, 8937-8941.
2 H.-P. Zhou, H.-S. Wu, J. Shen, A.-X. Yin, L.-D. Sun and C.-H. Yan, *J. Am. Chem. Soc.,* 2010, **132**, 4998-4999.
3 X. Wang, D. Liu, S. Song and H. Zhang, *J. Am. Chem. Soc.,* 2013, **135**, 15864-15872.
4 K. An, S. Alayoglu, N. Musselwhite, S. Plamthottam, G. Melaet, A. E. Lindeman and G. A. Somorjai, *J. Am. Chem. Soc.,* 2013, **135**, 16689-16696.
5 P. Xu, R. Yu, H. Ren, L. Zong, J. Chen and X. Xing, *Chem. Sci.*, 2014, **5**, 4221-4226.
6 T. Kayama, K. Yamazaki and H. Shinjoh, *J. Am. Chem. Soc.,* 2010, **132**, 13154-13155.
7 F. Liang, Y. Yu, W. Zhou, X. Xu and Z. Zhu, *J. Mater. Chem. A*, 2015, **3**, 634-640.
8 H.-X. Mai, L.-D. Sun, Y.-W. Zhang, R. Si, W. Feng, H.-P. Zhang, H.-C. Liu and C.-H. Yan, *J. Phys. Chem. B,* 2005, **109**, 24380-24385.
9 K. M. Bratlie, H. Lee, K. Komvopoulos, P. Yang and G. A. Somorjai, *Nano Lett.,* 2007, **7**, 3097-3101.
10 T.-S. Nguyen, G. Postole, S. Loridant, F. Bosselet, L. Burel, M. Aouine, L. Massin, P. Gélin, F. Morfin and L. Piccolo, *J. Mater. Chem. A*, 2014, **2**, 19822-19832.
11 X. Wang, D. Liu, J. Li, J. Zhen, F. Wang and H. Zhang, *Chem. Sci.*, 2015, **6**, 2877-2877.
12 P. Lu, B. Qiao, N. Lu, D. C. Hyun, J. Wang, M. J. Kim, J. Liu and Y. Xia, *Adv. Funct. Mater.,* 2015, **25**, 4153-4162.
13 J. Ke, J.-W. Xiao, W. Zhu, H. Liu, R. Si, Y.-W. Zhang and C.-H. Yan, *J. Am. Chem. Soc.*, 2013, **135**, 15191-15200.
14 N. Singhania, E. A. Anumol, N. Ravishankar and G. Madras, *Dalton. Trans.,* 2013, **42**, 15343-15354.
15 S. Agarwal, L. Lefferts, B. L. Mojet, D. A. J. M. Ligthart, E. J. M. Hensen, D. R. G. Mitchell, W. J. Erasmus, B. G. Anderson, E. J. Olivier, J. H. Neethling and A. K. Datye, *ChemSusChem,* 2013, **6**, 1898-1906.
16 F. Zhu, G. Chen, S. Sun and X. Sun, *J. Mater. Chem. A,* 2013, **1**, 288-294.
17 X. Ji, S. Evers, K. T. Lee and L. F. Nazar, *Chem. Commun.,* 2010, **46**, 1658-1660.
18 X. W. Lou, L. A. Archer and Z. Yang, *Adv. Mater.,* 2008, **20**, 3987-4019.
19 K. Zhou, Z. Yang and S. Yang, *Chem. Mater.,* 2007, **19**, 1215-1217.
20 H. J. Fan, U. Gosele and M. Zacharias, *Small,* 2007, **3**, 1660-1671.
21 D.-F. Zhang, L.-D. Sun, C.-J. Jia, Z.-G. Yan, L.-P. You and C.-H. Yan, *J. Am. Chem. Soc.,* 2005, **127**, 13492-13493.
22 G. Chen, C. Xu, X. Song, S. Xu, Y. Ding and S. Sun, *Cryst. Growth Des.,* 2008, **8**, 4449-4453.
23 L. Li, A. H. Larsen, N. A. Romero, V. A. Morozov, C. Glinsvad, F. Abild-Pedersen, J. Greeley, K. W. Jacobsen and J. K. Norskov, *J. Phys. Chem. Lett.,* 2013, **4**, 222-226.
24 R. Ouyang, J.-X. Liu and W. X. Li, *J. Am. Chem. Soc.,* 2013, **135**, 1760-1771.
25 S. B. Simonsen, I. Chorkendorff, S. Dahl, M. Skoglundh, J. Sehested and S. Helveg, *J. Am. Chem. Soc.,* 2010, **132**, 7968-7975.
26 S. Song, X. Wang and H. Zhang, *NPG Asia Materials,* 2015, **7**, e179.
27 N. Zhang and Y.-J. Xu, *Chem. Mater.,* 2013, **25**, 1979-1988.
28 K. Yoon, Y. Yang, P. Lu, D. Wan, H.-C. Peng, K. S. Masias, P. T. Fanson, C. T. Campbell and Y. Xia, *Angew. Chem. Int. Ed.,* 2012, **51**, 9543-9546.
29 C. Chen, X. Fang, B. Wu, L. Huang and N. Zheng, *ChemCatChem,* 2012, **4**, 1578-1586.
30 G. Chen, F. Rosei and D. Ma, *Adv. Funct. Mater.,* 2012, **22**, 3914-3920.
31 G. Chen, C. Xu, X. Song, W. Zhao, Y. Ding and S. Sun, *Inorg. Chem.,* 2008, **47**, 723-728.
32 G. Chen, S. Sun, X. Sun, W. Fan and T. You, *Inorg. Chem.,* 2009, **48**, 1334-1338.
33 G. K. Wertheim, S. B. Dicenzo and S. E. Youngquist, *Phys. Rev. Lett.,* 1983, **51**, 2310-2313.
34 J. Zarraga-Colina and R. M. Nix, *Surf. Sci.* 2006, **600**, 3058-3071.
35 Y. Zhou, J. M. Perket and J. Zhou, *J. Phys. Chem. C,* 2010, **114**, 11853-11860.
36 H. J. Freund, *Angew. Chem. Int. Ed. Engl.,* 1997, **36**, 452-475.
37 V. Matolín, M. Cabala, I. Matolínová, M. Škoda, M. Václavů, K. C. Prince, T. Skála, T. Mori, H. Yoshikawa, Y. Yamashita, S. Ueda and K. Kobayashi, *Fuel Cells,* 2010, **1**, 139-144.
38 G. N. Vayssilov, Y. Lykhach, A. Migani, T. Staudt, G. P. Petrova, N. Tsud, T. Skála, A. Bruix, F. Illas, K. C. Prince, V. Matolín, K. M. Neyman and J. Libuda, *Nat. Mater.,* 2011, **10**, 310-315.
39 O. S. Alexeev, F. Li, M. D. Amiridis and B. C. Gates, *J. Phys. Chem. B,* 2005, **109**, 2338-2349.
40 R. Siburian and J. Nakamura, *J. Phys. Chem. C,* 2012, **116**, 22947-22953.
41 J. Ke, W. Zhu, Y. Jiang, R. Si, Y.-J. Wang, S.-C. Li, C. Jin, H. Liu, W.-G. Song, C.-H. Yan and Y.-W. Zhang, *ACS Catal.,* 2015, **5**, 5164-5173.

42 F. Lin, D. T. Hoang, C.-K. Tsung, W. Huang, S. H.-Y. Lo, J. B. Wood, H. Wang, J. Tang and P. Yang, *Nano. Res.,* 2010, **4**, 61-71.

43 A. C. Mak, C. Yu, J. C. Yu, Z. Zhang and C. Ho, *Nano. Res.,* 2008, **1**, 474-482.

44 D. Pierre, W. Deng and M. Flytzani-Stephanopoulos, *Top. Catal.,* 2007, **46**, 363-373.

45 A. Martínezarias, J. M. Coronado, R. Cataluña, J. C. Conesa and J. Soria, *J. Phys. Chem. B,* 1998, **102**, 4357-4365.

46 P. Bera, A. Gayen, M. S. Hegde, N. P. Lalla, L. Spadaro, F. Frusteri and F. Arena, *J. Phys. Chem. B,* 2003, **107**, 6122-6130.

Graphical Abstract

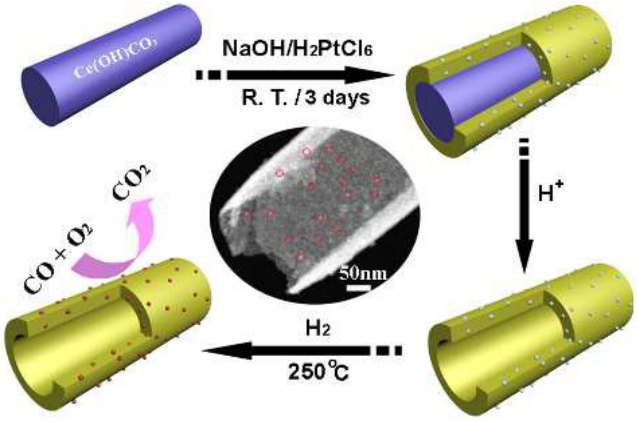

The good balance of catalytic activity and thermal stability is technologically crucial yet challenging problem for noble metal based catalysts. Herein, ceria nanotube-embedded ultra-small Pt nanoparticle (NP) catalyst was synthesized by means of an interfacial reaction in the absence of any surfactants or surface modification. Due to the ultra-small size of catalytically active Pt NPs and the extensive contact between Pt and ceria, the catalyst exhibits remarkable catalytic activity toward CO oxidation. More importantly, it shows superior thermal stability not only for Pt NPs but also for ceria, even at 700 °C.